Talanta 190 (2018) 158–166

Contents lists available at ScienceDirect

Talanta

journal homepage: www.elsevier.com/locate/talanta

Innovative unattended SEM-EDS analysis for asbestos fiber quantification

Roberto Cossio[a,b], Carlo Albonico[c], Andrea Zanella[c], Silvia Fraterrigo-Garofalo[d], Chiara Avataneo[e], Roberto Compagnoni[a,b], Francesco Turci[a,d,*]

[a] "G. Scansetti" Interdepartmental Center for Studies on Asbestos and Other Toxic Particulates, University of Torino, Torino, Italy
[b] Department of Earth Sciences, University of Torino, Via Valperga Caluso 35, I-10125 Torino, Italy
[c] Regional Agency for the Protection of the Environment of Valle d'Aosta (ARPA VdA), I-11020 Saint Christophe, Aosta, Italy
[d] Department of Chemistry, University of Torino, Via P. Giuria, 7, I-10125 Torino, Italy
[e] Gi-RES S.r.l., Geological Risk Analysis, Torino, Italy

ARTICLE INFO

Keywords:
SEM-EDS
Automatic image analysis
Asbestos quantitative measurement
Naturally occurring asbestos
Asbestos detection limit

ABSTRACT

Scanning electron microscopy with energy dispersive spectrometry (SEM-EDS) is the only affordable analytical technique that can discriminate both morphology and elemental composition of inorganic fibers. SEM-EDS is indeed required to quantify asbestos in confounding natural matrixes (e.g. ophiolites), but is also time-consuming, operator dependent, and strongly relies on the stochastic distribution of the fibers on the filter surface. The balance between analytical time/cost and the method sensibility allows only about 0.5% of the filter to be analyzed, strongly affecting the statistical significance of results. To improve sensitivity and precision and enhance productivity, an unattended quantitative measurement of the asbestos fibers by SEM-EDS is proposed. The method identifies the particle shape first and determines their chemical composition later, saving EDS analytical time. Our approach was tested on four asbestos standards and the relative error on replicated measurements was < 10%. The proposed unattended method quantifies asbestos in natural confounding matrix, also with a very low asbestos content.

1. Introduction

The release of Natural Occurring Asbestos (NOA) fibers into the air from rocks and soils during human activities or natural weathering poses a potential risk to human health [1–4]. Ophiolites, which are sections of the Earth's oceanic lithosphere, including both the oceanic crust and the underlying uppermost mantle, uplifted and exposed above continents by tectonic processes, are the most significant sources of NOA. Among the different types of rocks making up the ophiolitic sequences, green-colored serpentinites derived from the hydration of the upper mantle peridotites commonly occurs. Serpentinites often include veins filled with chrysotile and/or tremolite asbestos and are the main source of NOA in Europe and North America. Excavation, tunneling, construction, and generally all anthropic activities carried out in ophiolitic rocks may occasionally release NOA and demand fast and reliable methods for the quantitative detection of asbestos [5]. Unfortunately, unambiguous detection of asbestos in the natural environment is not trivial, especially when the fibers occur at low concentration. Airborne particle monitoring in natural environment typically shows several elongated mineral particles (EMP) other than asbestos, including fibrous calcium carbonate, plagioclase, gypsum, and synthetic fibers such as titanium dioxides, titanates and aluminum-silicates [4,6,7]. These fibers share with asbestos the high aspect ratio, often greater than 10:1, but elemental or structural analysis often couple with electron microscopies (EM) may conveniently discriminate EMPs from asbestos. The analysis of NOA in soil and rock is further complicated by the host matrix often sharing with asbestos the very same elemental composition and/or crystallographic features. Therefore, the analytical approaches commonly adopted for measuring asbestos in artificial materials, including X ray Powder Diffractometry (XRPD) and Infrared Spectroscopy (FTIR) are not able to discriminate the non-fibrous matrix from asbestos in natural samples. Also XRPD and FTIR analytical sensibility is limited to asbestos concentration > 1% [8], unless sample enrichment is performed [9]. In this latter case, a limit of detection below 0.1% was achieved, but the method was still not able to discriminate asbestos from its confounding host-matrix.

Abbreviations: EDS, energy dispersive spectroscopy; EM, electron microscopy; EMP, elongated mineral particles; FTIR, Fourier transformed infrared spectroscopy; NOA, naturally occurring asbestos; PCM, phase-contrast microscopy; PLM, polarized light microscopy; SEM, Scanning Electron Microscopy; TEM, Transmission Electron Microscopy; XRPD, X-ray Powder Diffractometry

* Corresponding author at: Department of Chemistry, University of Torino, Via P. Giuria, 7, I-10125 Torino, Italy.
E-mail address: francesco.turci@unito.it (F. Turci).

https://doi.org/10.1016/j.talanta.2018.07.083
Received 9 May 2018; Received in revised form 23 July 2018; Accepted 26 July 2018
Available online 27 July 2018
0039-9140/

Among the available techniques, only microscopies indeed discriminate between fibrous and non-fibrous form of the very same mineral. Usually, asbestos fibers are collected (airborne) or deposited (waterborne or rock/soil) on a porous membrane which is observed. Fibers on the membrane are counted or measured to obtain a quantification of asbestos. However, light microscopies, including polarized light microscopy (PLM) and phase-contrast microscopy (PCM), cannot resolve thin asbestos fibers and occasionally yields inaccurate results due to presence of confounding minerals. Electron microscopies (EM) are often preferred due to their higher spatial resolution and depth-of-field. Among EMs, Transmission Electron Microscopy (TEM) offers the highest resolution and the most accurate fiber identification, but requires long analysis time for a statistically relevant quantitative analysis. In addition, TEM set-up and management costs are very high with respect to Scanning Electron Microscopy (SEM). In this work, we focused on SEM coupled with Energy Dispersive Spectroscopy (EDS). With higher operational speed and lower costs, conventional SEM-EDS provides a fairly

good resolution and is today a common tool in health and safety laboratories to analyze airborne, waterborne and rock and soil-dispersed NOA. Nevertheless, SEM and microscopies in general, may yield biased results based on the subjective opinion of the operator [10] who has to discriminate manually asbestos from non-asbestos minerals. Furthermore, using serial dilutions, it was demonstrated that operators tend to overestimate fiber count on low-concentrated samples and underestimate it on high-concentrated ones [11]. Generally, asbestos quantification via optical or electron microscopies could largely be improved in terms of analytical productivity and result reproducibility if a non-biased approach is developed [12]. Several papers on the automatic measurement of asbestos with light microscopy were lately published [13,14], but currently none of them were developed to be used with electron microscopy. The main issues that automated analysis has to face are due to the fact that fibers can exist as curved rods, complex bundles and agglomerates of fibers, and stumpy particles. Furthermore, only a small portion of the filter is investigated, and the inhomogeneous distribution of asbestos fiber on the filter often yields high analytical error. Specifically, the visible area of a conventional filter for asbestos analysis ranges from 254 to 385 mm^2 on a conventional 1-in. diameter filter, and the observation of thousands of fields is required to scan the entire membrane. To keep the measurement time acceptable, the observation of an area of ca. 1 mm^2 is usually required in many national and international procedures. According to the Italian law, very similar to ISO 14966:2002, only a small portion (0.37 ÷ 0.57%) of the entire filter is observed and the asbestos concentration per surface unit is extrapolated to the entire filter. It is generally assumed that the particle spatial distribution on the filter obeys to a two-dimensional Poisson distribution and in turn, the number of microscopic fields examined directly determines the statistical significance of the measure. However, NOA, in which several events concur to produce fibers, are morphologically extremely heterogeneous and the wide range of fiber size may require more than 100 fields in order to get a reliable quantification of asbestos. It was shown that inter-laboratory SEM analyses on asbestos-bearing rocks (mine tailings) produce very dispersed results [15]. Currently SEM quantitative analysis is indeed limited to the observation of 100 microscopic fields or ca. 1 mm^2 due to the time-consuming visual inspection of each microscopic filed, but the statistical significance of the measurement could be improved dramatically if a larger number of fields were analyzed. To take advantage of the high resolution of SEM and virtually being able to examine the whole membrane, a reliable unattended asbestos fiber counting method based on SEM-EDS capable of improve precision and sensitivity of asbestos detection is here proposed.

The aim of this work is to reduce the analytical time/cost for asbestos measure, allowing a more robust quantification to be obtained. We estimated precision and accuracy of SEM-EDS analysis of asbestos in complex matrixes such as natural ophiolitic rock and described the first unattended quantitative measurement of naturally occurring asbestos fibers by SEM-EDS method. The proposed algorithm identifies the particle shape first and determines NOA chemical composition later cross validating the correct assignment of each fiber detected on the filter.

2. Experimental

2.1. Asbestos standards

Asbestos standards were from UICC repository [16] and used without further modifications. UICC standard physico- and crystallochemical characterization were refined by Kohyama and coworkers [17]. The ideal formulas of the minerals are the following:

- UICC amosite (amphibole, fibrous grunerite): $Fe_7Si_8O_{22}(OH)_2$
- UICC crocidolite (amphibole, fibrous riebeckite): $Na_2(Fe_3^{2+}Fe_2^{3+})Si_8O_{22}(OH)_2$
- UICC chrysotile (serpentine, fibrous): $Mg_3(Si_2O_5)(OH)_4$

To complete the set of environmentally relevant asbestos mineral, a sample of fibrous tremolite, thoroughly characterized in previous works [18–20], was used:

- Susa tremolite (fibrous amphibole, from Susa Valley, Italy): $Ca_2Mg_5Si_8O_{22}(OH)_2$

2.2. Naturally occurring asbestos samples

To assess the applicability of the unattended method on real samples in a complex matrix, a set of NOA-rich soils were collected and characterized. Detailed petrological characterization of the NOA samples is reported in Section S1, Supporting information.

- NOA1: coarse-grained damp deposit containing pebbles of antigorite-serpentinite with veins of both fibrous tremolite and chrysotile in the approximate ratio 90:10). Damp deposit of Illes Neuves nearby Salbertrand, Susa Valley, Western Alps, Italy. The sample is characterized by a high asbestos content.
- NOA2: coarse-grained damp deposit containing pebbles of antigorite-serpentinite with veins of both fibrous tremolite and chrysotile (approx. in the ratio 90:10). Damp deposit of Illes Neuves nearby Salbertrand, Susa Valley, Western Alps, Italy. The sample is characterized by a low asbestos content.
- NOA3: Foliated antigorite Serpentinite containing undeformed mm-thick veins of asbestos. Near the village of Lanzada, Val Malenco, Sondrio Province, Central Alps, Italy.

2.3. Instruments

The SEM used was a Zeiss EVO MA10 with W or LaB_6 source, equipped with an EDS (Oxford Instruments Inca Energy 250, X-Act SDD detector and the Feature package software).

2.4. Sample preparation

2.4.1. Preliminary sample preparation

Rock samples were preliminary grinded at the CNR – Institute of Environmental Geology and Geoengineering, Monterotondo, Rome, using a Jaw Cruscher Retsch BB 200 equipped with stainless steel breaking jaws and variable openings to obtain a size reduction from < 90 mm down to < 2 mm. A Retsch PT 100 Rotary Sampler Divider, equipped with 8 sample vessels (holding capacity 250 ml and Driving Head Speed 110 RPM), was used to obtain a representative aliquot of sample. The sample was screened using a sieve with opening size of 1 mm and it was divided again with the rotary sample divider. The coarse powder was wet-milled in isopropyl alcohol (liquid/solid ratio of 1:1) with a Bleuler Rotary Cup Mill equipped with Chrome Steel

container sets with a holding capacity of 100 ml and 900 RPM motor speed. The suspension was then transferred to a non-ventilated oven set at 90 °C and isopropyl alcohol evaporated for ca. 1 h. A granulometry of the particulate lower than 100 μm was achieved with a grinding-time of 8 s.

2.4.2. Membrane preparation for SEM fiber measure

About 5 mg of the fine powder were weighed and suspended in 200 ml of a 0.1% dioctyl-sulfosuccinate solution, prepared in filtered (0.22 μm porosity) deionized water. To prevent fiber sedimentation and allow fiber disaggregation, the dispersion was magnetic stirred for 20 min. Using a vacuum filtration system, a proper amount of the suspension was transferred on a polycarbonate membrane (2.5 cm diameter, 0.8 μm porosity) to deposit ca. 0.1 mg of the sample on the membrane. The membrane was dried in a non-ventilated oven at 90 °C and mounted on an aluminum sample holder for electron microscopy. Graphite tape was used to hold the membrane on the sample holder and graphite bridges were used to connect the filter edge with the sample holder to improve electron transfer and prevent sample overcharge. The membrane was coated with a 30 nm thick carbon layer by evaporation.

3. Results and discussion

3.1. Definition of SEM instrumental parameters

To characterize the asbestos fibers by means of Scanning Electron Microscopy, it is of paramount importance to determine accurately the volume from which the analytical signals are produced. For such a reason, the excitation range of the primary electron probe ($\mathbf{R_{KO}}$) within the sample was simulated for fibers with different average atomic numbers ($\mathbf{Z_{mean}}$) and the SEM instrumental parameters fine-tuned for the asbestos analysis (see Supporting information, Section S2).

3.2. Image binarization and threshold selection

The first step, generally referred to as thresholding (TH), is the conversion of the analogical image formed by a wide range of gray levels (in the present case an 8-bit gray-scale image allows 256 different shades of gray to be recorded) to a discrete (binary, 1-bit) image, goaled at unambiguously defining the shape of the examined particle/object. Thresholding is normally performed by an operator, using the morphological SE image. For such a reason, with an automatic counting method it is essential to store this image for validating an *a posteriori* assignment of each object to a specific fiber class. In conditions of electron beam stability, the most rigorous approach for polished samples requires – at any operating conditions – two preliminary measurements on two reference samples to evaluate (i) the X-ray photons production (Quant Optimization) and (ii) the gray levels of the BSE image. Referring to the calculated Z_{mean} values (see Table S1, Supporting information), a multi-standard reference set with atomic numbers encompassing the average Z of asbestos was prepared, embedded in resin, and polished. Co and Ti were used for the Quant Optimization of EDS analysis at two different acceleration voltages, namely 20 and 10 KeV, and Si and Al_2O_3 for calibrating maximum and minimum gray levels, respectively. This standard set was permanently mounted on the SEM sample holder and its position on the SEM stage stored, in order to easily rerun the calibration procedure during the analysis. The gray calibration was performed adjusting the brightness and contrast of the BSE signal obtained from the Si (high level) and Al_2O_3 (low level) standard (see section S2.1, Supporting information).

Under these conditions, it was possible to obtain a gray-calibrated image of an asbestos reference standard and perform a meaningful image binarization. Fig. 1 reports the SE (A) and BSE (B) images of the amosite standard taken at 2000 x magnification, the relative BSE gray level histogram (C), and the binary image obtained from BSE image after the threshold calibration (D). The gray level histogram of BSE image shows a sharp peak close to level 0 due to the low-Z polycarbonate filter. The peak at higher gray-level (> 200) is due to the analyzed fibers. For a correct separation of the fibers of interest from any other material occurring on the surface of the filter, including the filter itself, a proper selection of the two upper and lower threshold levels (the two blue lines in Fig. 1C) has to be carried out manually. To take into account the whole range of the fiber diameter and asbestos Z_{mean} values (Table S1, Supplementary material), a standard set for each mineral species of interest was used. Generally, more than one threshold set must be used in order to optimize the detection accuracy. The threshold calibration must be performed at the very same analytical conditions used for the unknown sample.

3.3. Optimization of the analytical conditions

Several optimizations were performed to achieve the best acquisition conditions (see section S3, Supporting information). Both W and LaB_6 were used as the electron beam source. The LaB_6 cathode has a higher brightness and allows a better spatial/optical resolution, but suffer of a slightly lower stability with respect to the W source. The LaB_6 source was chosen, with beam instability being compensated by a more frequent calibration of the reference gray levels. The electron beam energy was 10 keV as this value represents the best compromise between the small volume to be analyzed and the energy necessary to excite the elements of interest. With the EDS analyses a moderately high I_{probe} gives a higher counting efficiency, reducing the counting time. At 2000x magnification, the size of a single microscopic field (E_0 = 10 keV, WD = 12 mm) is 140 × 100 μm. When a digital image width of 1024 pixels was used, the smallest detected feature was 0.28 μm. A 2048-pixel image was also used and the smallest feature detectable was 0.14 μm, but the acquisition time increases consequently. The acquisition time of a field could be dramatically reduced by performing a 2-step acquisition routine. In Step 1 (fast scan), a whole field is scanned with a short dwell time. In the Step 2 (slow scan), a longer dwell time is used to image at high signal-to-noise ratio only the particles of interest that were recognized during Step 1. Particles were analyzed by a morphometric filter that discriminates among fibrous and non-fibrous objects. The EDS spectra were acquired only for the “fibers”, thus further saving analytical time. To compensate for the scanning shift between the two scans at different speed, a number of horizontal extra pixels before and after each fiber (“Leading” and “Trailing”) were added in order to prevent an incomplete measurement of the fiber. The 2-step routine relies on the application of the morphometric and/or compositional filters in order to acquire and store data only from asbestos fibers and disregard the rest.

3.4. Fiber counting and morphometry

To obtain statistically significant results, fiber counting on a small portion of the filter requires that particulate matter on the filter follows a two-dimensional Poisson distribution (Supporting information, Section S3.1). Conventional microscopic analyses cannot be normally replicated due to the high analytical time required for fiber count and a limited portion of the filter can be observed, usually the 0.5%. The statistical significance of the measure can only be estimated by calculating the confidence limits a_1 and a_2 (Section S3.1). The proposed unattended method allows the measurement to be repeated and statistical significance directly tested (Section S3.2).

Fiber morphology, including length, width, and aspect (length/width) ratio, is currently used to analytically discriminate between asbestiform and non-asbestiform minerals. However, taxonomic confusion and lack of unambiguous definitions for fibers, especially the discrepancies between mineralogical and regulatory definition, makes the asbestos quantitative analysis quite subjective and urge the scientific community to reach a clear consensus [7,21–23]. In this confused scenario, we decided to introduce flexible morphometric parameters

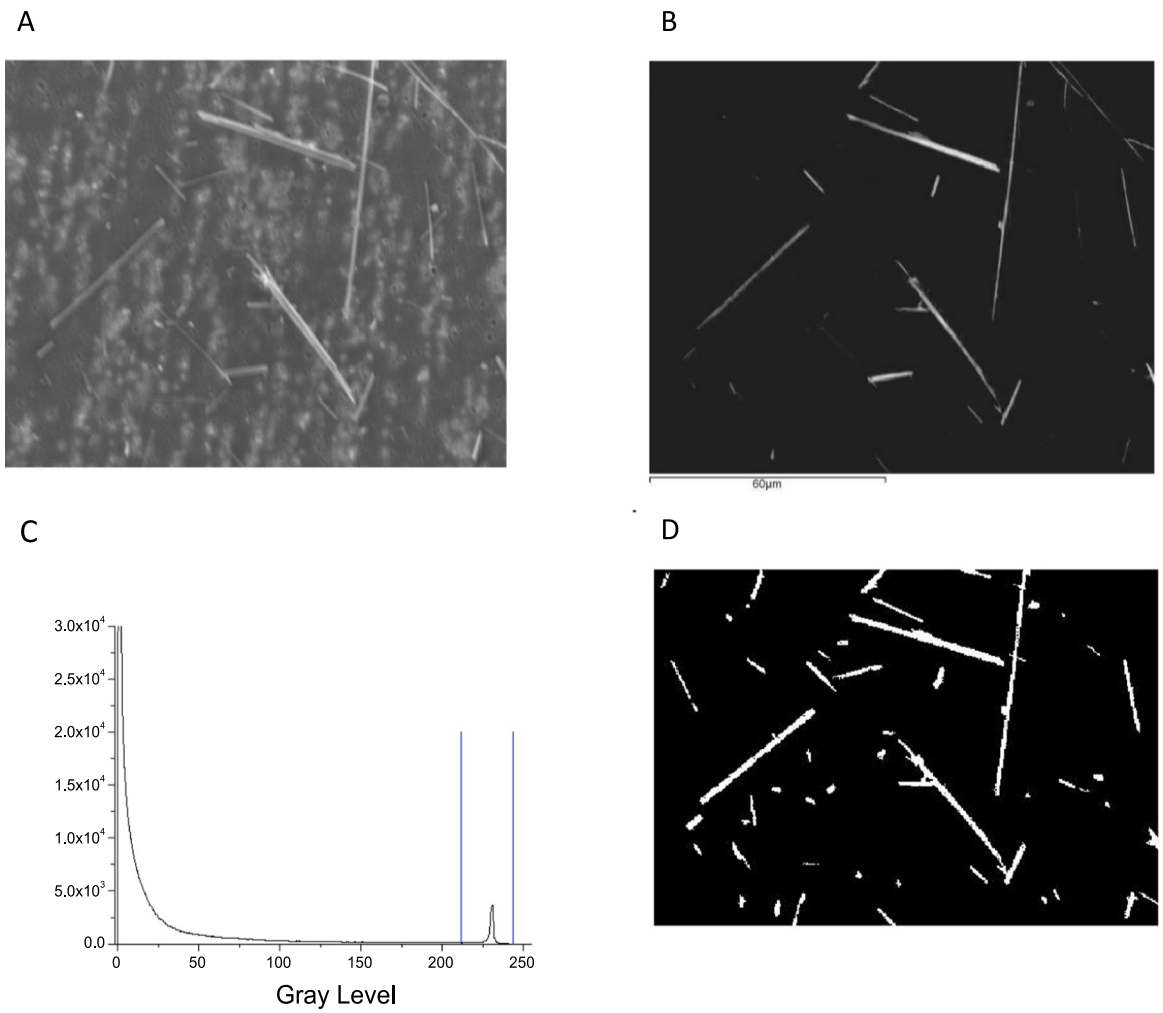

Fig. 1. Amosite standard (A) SE image (2000x magnification), (B) BSE image, (C) gray level histogram of BSE image in B, and (D) binary image of amosite after thresholding (TH).

that could be adapted easily to all current and forthcoming regulatory definitions of fiber, or even use different figures for airborne, waterborne, and massive samples. Furthermore, during the automatic analysis several morphometric parameters were calculated for each fiber, thus gaining a more exhaustive description of the morphology of the object than the two parameters (length and width) that are currently measured. The set of the morphological parameters that were useful in asbestos/non-asbestos discrimination is reported in Table S3 (Section S4, Supporting information). Usually, automatic image analysis uses maximum and minimum Feret diameters to approximate particle Length and Width, respectively. In the case of individual, straight, and regular fibers, e.g. amphiboles, Feret diameters can correctly discriminate among asbestiform and non-asbestiform particles. Conversely, curled and irregular fibers, e.g. chrysotile (Fig. 2A and B), but also amphiboles superimposed to other particles (Fig. 2C), are subject to a width overestimation when Feret parameters are used. This in turn produced a consequent unacceptable underestimation of the particle "aspect ratio" (red dotted rectangles, in Fig. 2) and misleading volume calculation.

To avoid the error due to the Feret method, we approximated the fiber with an "equivalent rectangle" (ER) that shares the area (A) and perimeter (P) with each particle, rendering straightforward the measurement of length (L) and width (W). To obtain ER, the equivalence between P and A of the particle and the rectangle (Fig. 2, green line) leads to the quadratic equation:

$$R_{1,2} = \frac{P \pm \sqrt{P^2 - 16A}}{4}$$

where P and A are the perimeter and area, and the two $R_{1,2}$ solutions being length (L_{eq}) and width (W_{eq}) of the ER, respectively. For chrysotile fibers reported in Fig. 2A and B, the ER and the Feret methods yielded an aspect ratio of 158.3 and 3.2, and 114.6 and 3.8, respectively (morphometric measures are comparatively reported in Tab S5, Supporting information). This result clearly highlights how the ER method more suitably approximates the fibrous geometry of asbestos with respect to Feret diameters. This approach is helpful even when the fiber is not perfectly regular (Fig. 2C and D) and was adopted for the following experimental evaluation of the method. The four asbestos reference samples were placed on filters and analyzed. In the case of a pure asbestos sample, the number of objects counted should correspond to the number of morphologically valid fibers. A comparative fiber count is reported in Table 1.

After the use of the morphometric filter set to World Health Organization's definition of fiber (Tab. S4, Supporting information), the Particle Number enumerates all the objects counted during membrane analysis, and Fiber Number reports the objects classified as "fibers" by the Feret and ER methods. Clearly, the ER method largely improves fiber recognition, up to 94% for crocidolite. Furthermore, ER allows multiple tangled fibers to be transformed into a single equivalent fiber, that shares Area and Perimeter with the tangled group (Fig. 2D). The ER method can conveniently approximate also chrysotile bundles that are

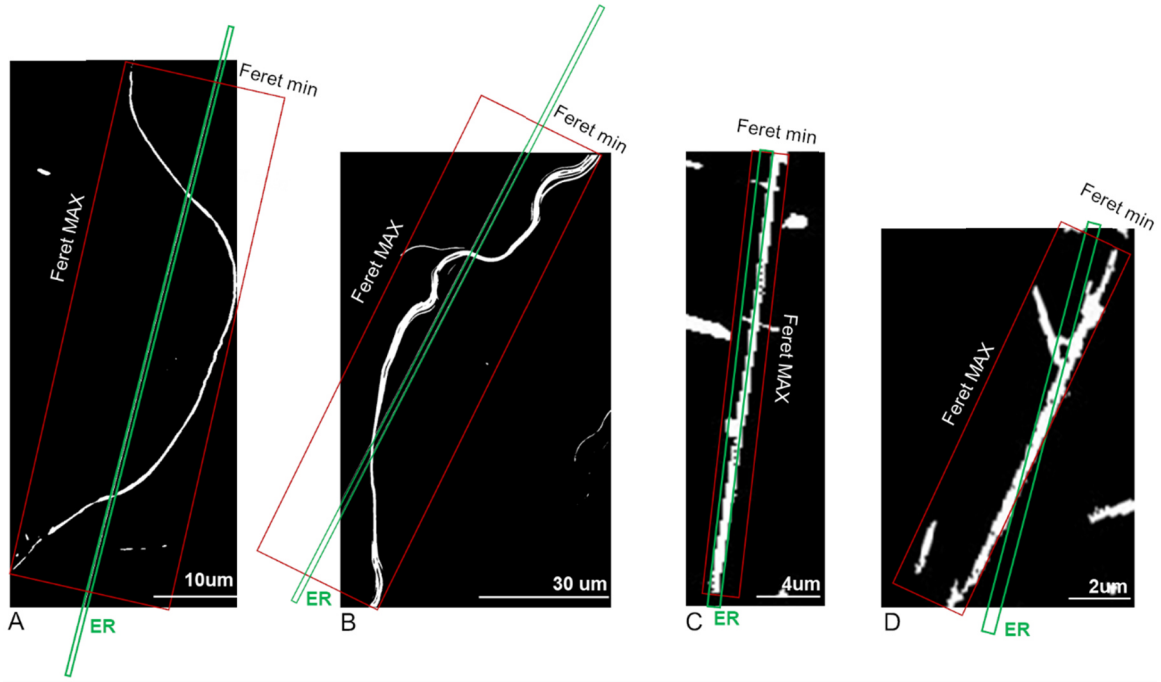

Fig. 2. Binary images of curled chrysotile (A and B) and amosite (C and D) fibers. Feret diameters (dotted red rectangle) and the equivalent rectangle (ER, green) are superimposed to binary images to emphasize the morphological discrepancy between the two approximations. (For interpretation of the references to color in this figure legend, the reader is referred to the web version of this article.).

Table 1
Fiber classification using Feret and ER parameters under morphological constrain defined by WHO for respirable fiber (Tab. S4, Supporting information).

	Morphometric method	Particles classified as "fibers"	Particles counted	%
Chrysotile	Feret diameters	416	834	49.88
	ER	656		78.66
Tremolite	Feret diameters	670	1165	57.51
	ER	1094		93.91
Amosite	Feret diameters	1145	2135	53.63
	ER	1907		89.32
Crocidolite	Feret diameters	884	2296	38.50
	ER	2160		94.08

possibly the most difficult object to approximate due to their low aspect ratio and shape discontinuity. Few examples are reported in Fig. 3.

Generally, the ER area can be compared to the real area of the bundled, tangled fibers and the A_{ER}/A_{real} percentage calculated. A 100% score represents the ideal case of a single fiber with perfect cylindrical shape. Practically, a score higher than 80% indicates a single straight amphibole fiber, while a lower score highlights either a group of fibers or a curled fiber. These low-scored fibers, generally less than 10% of the fibers on filter, may be re-processed *a posteriori* to confirm manually the count and object dimension by analyzing SE, BSE images, and the EDS chemical data.

To verify the reliability of the ER approximation, especially for fibers with a difficult morphology to be approximated, including extremely curled, split, open, aggregated, cross-cut fibers, bundles, and fibers with a variable diameter along fiber axis, a repository of gray-scale images, superimposed to their approximated ER was prepared for both chrysotile and tremolite. Two sets of 10 representative images of chrysotile and tremolite fibers are reported in the Section S5 of the Supporting information, Figs. S7, S8, respectively. Aspect ratio and weight of each selected fiber were comparatively measured both automatically by using ER approximation, and manually by a trained operator. The diameter of each fiber was measured in several slightly different points across the fiber to take into account the subjective bias affecting the manual measurement among different operators. The comparative evaluation of aspect ratios (A and B) and weights (C and D) of the selected chrysotile (A and C) and tremolite (B and D) fibers, automatically (red stars) and manually calculated (empty symbols), is reported in Fig. 4. The aspect ratio evaluated via ER approximation showed a good correlation with the average value (horizontal black line) obtained by the operator for each chrysotile and tremolite fiber. Interestingly, the ER approximation yielded weight results that are even closer to the manual measures than AR values for both chrysotile and tremolite. The fiber weight automatically measured for chrysotile was generally higher than the weight obtained by the operator. The observed underestimation of the fiber weight is likely due to the curled aspect of chrysotile that may impair a proper measure of fiber length with a polygonal open line, manually. The ER approximation instead takes into consideration both the area and the perimeter of chrysotile fiber, thus bi-dimensionally approximating the actual shape with a greater accuracy than what the human operator does. The discrepancy between the two approaches was even lower for the set of tremolite. When tremolite fiber width may not be easily measured, such as in highly fractured fragments (e.g. Trm_10 in Fig. S8, Supporting information), the operator is prone to produce biased results, choosing subjectively among wider or narrower fiber diameters. In such cases, ER approximation may again improve accuracy of the measure by re-creating a new ideal rectangular fiber that shares with the real fiber the area (all and only the white pixels on the binary image) and the perimeter.

An aspect ratio analysis on a large set of tremolite fibers was also carried out to show how automatic analysis may discriminate among asbestiform and non-asbestiform minerals. The proposed automatic system may indeed take advantage of the stronger statistically significance of the results due to the tremendous number of particles that may be measured during a conventional analysis. A dataset of ca. 1000 tremolite particles and fibers was analyzed and the aspect ratio frequency plot calculated (Section S7, Supporting information). The experimental plot was fitted with a multi-curve unconditioned fitting

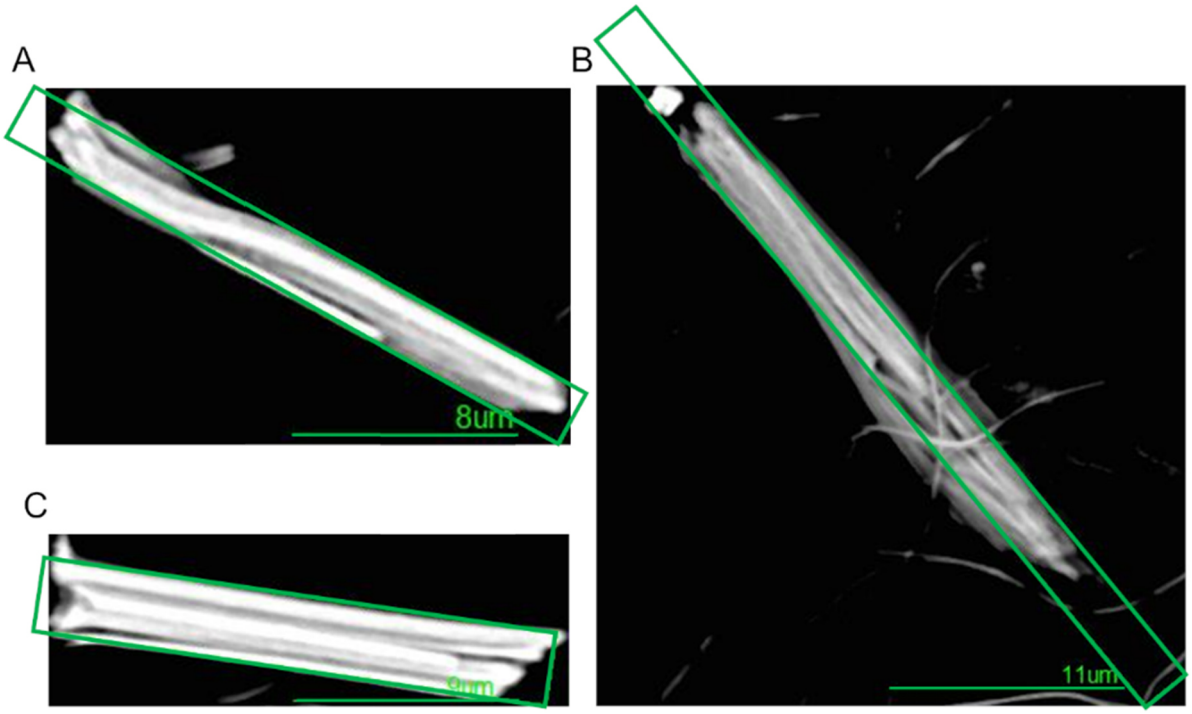

Fig. 3. Representative images of three chrysotile bundles, approximated by ER.

procedure and four peaks, corresponding to four classes of tremolite particles, were detected (Fig. S12, Supporting information). We showed that a mixed sample of asbestiform and non-asbestiform tremolite may be properly sorted out in classes on the basis of the aspect ratio. The particle classes encompassed: 1) non-asbestiform tremolite particles derived from crushing of a former prismatic crystal; 2) elongated, acicular tremolite crystals with low AR; 3) fibrous/asbestiform particles, including tremolite bundles of fibers; 4) asbestiform tremolite fibers with AR $>$ 10, characterized by a constant cross-section and a straight habit. The assignment of particles belonging to the second class, the so-called elongated or acicular particles, to asbestos or non-asbestos realm is not trivial and may be sorted out with a manual review of the dubious cases. The automated system may indeed be integrated with a machine-learning (ML) algorithm that learns from analyst how to discriminate among asbestiform and non-asbestiform elongated fibers/bundles. The automated analysis may be set to prompt the operator to recognize manually the particles of the second class, adopting a case-by-case safer approach. Furthermore, the ML approach could take advantage of many other image parameters, including gray-scale distribution and other geometrical parameters beyond length and diameter, including roughness, and gray-scale relative errors, that may help to discriminate among different objects. The ML algorithm will likely integrate morphometry with some unconventional non-morphological parameters, such as average gray value or standard deviation of the mean gray of the object pixels. In this respect, chrysotile bundles, likely showing a higher grayscale dispersion due to the irregular height of the bundle fibrils, could be discriminated from antigorite splinters, exhibiting a lower grayscale dispersion.

3.5. Elemental asbestos discrimination

To discriminate among asbestos fibers, element-specific compositional boundaries had to be defined unambiguously for each asbestos mineral. By using the method described in the Section S6, Supporting information, an EDS spectrum was acquired for each fiber type defined in Table 1. A dataset of quantitative EDS analyses was populated for each asbestos standard and reported as wt%, normalized. The histograms of the compositional distribution for the main elements of asbestos minerals were plotted and the distributions were fitted with a single Gaussian curve (Fig. S10, Supporting information). For each curve, the centroid $\pm$ 2σ was used to discriminate the compositional interval for each fiber of interest. The compositional boundaries obtained are reported in Table 2.

The application of the compositional filter slightly reduced the number of fibers passing the asbestos discrimination as expected by the 2σ-interval considered as acceptable. The average EDS analyses obtained for each standard (Tab. S7, Supporting information) were in agreement with quantitative compositional analysis of asbestos [24].

To check the power of EDS asbestos discrimination, a Principal Component Analysis (PCA) was carried out on the dataset containing the elemental analyses of the four asbestos standards. The first two principal components expressed the 92.25% of the cumulative variance of the sample and were reasonably used to represent the dataset (Tab. S8, Supporting information). The four asbestos standards were unambiguously discriminated by their chemical compositions plotted as PC1 vs. PC2 (Fig. 5). The PCA results indicate that this approach may also conveniently discriminate asbestos from other minerals that share with asbestos the fibrous habit.

3.6. Precision and accuracy evaluation of asbestos standards and real samples

To validate the automatic approach proposed, we replicated several automated measures to check the precision of the method with amosite and tremolite standards. We also evaluated the accuracy of our approach by comparing the result of automatic analysis with the results obtained with the conventional SEM-EDS analysis on three natural complex samples (NOA).

The evaluation of the precision, reported in Fig. 6 (raw data in Table S10, Supporting information), highlighted that method reproducibility is fairly high, with relative error on four replicates ranging from 6% to 11.5%, for amosite and tremolite, respectively.

To estimate the accuracy of the proposed method, three porous membranes loaded with NOA from complex matrices were analyzed in

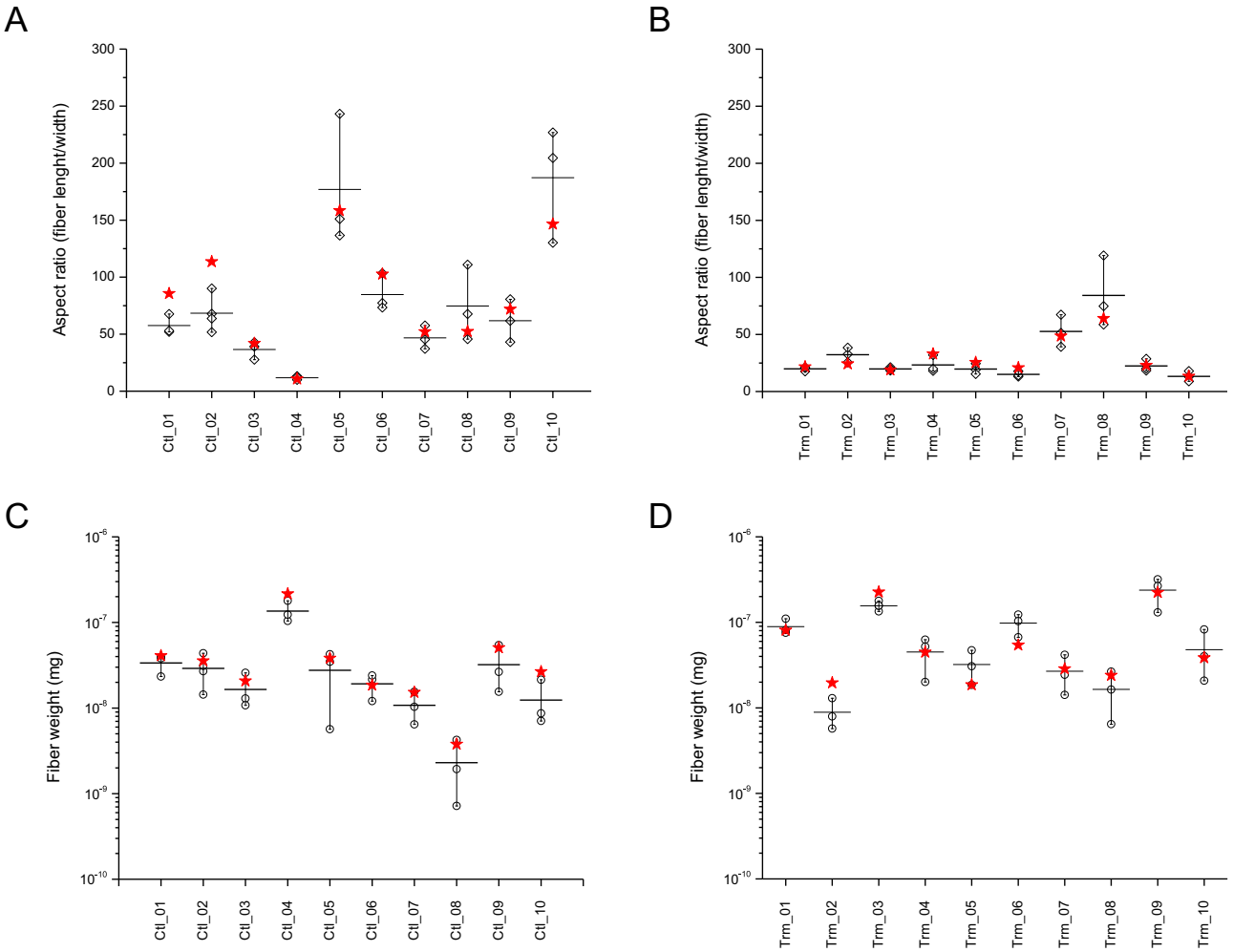

Fig. 4. Comparative evaluation of aspect ratios (A and B) and weights (C and D) of the 10 chrysotile (A and C) and tremolite (B and D) fibers automatically (red stars) and manually calculated (empty symbols).

Table 2
Compositional boundaries derived from the distribution of elemental analyses reported in Fig. S10, Supporting information.

	chrysotile		amosite		tremolite		crocidolite	
	Min	*Max*	*Min*	*Max*	*Min*	*Max*	*Min*	*Max*
Na (wt%)							4.55	10.23
Mg (wt%)	18.03	30.57	1.55	5.55	11.28	14.78		
Si (wt%)	15.78	27.92	19.52	30.71	22.78	28.14	19.26	25.25
Ca (wt%)					7.18	10.57		
Fe (wt%)			14.44	33.66			22.57	32.74

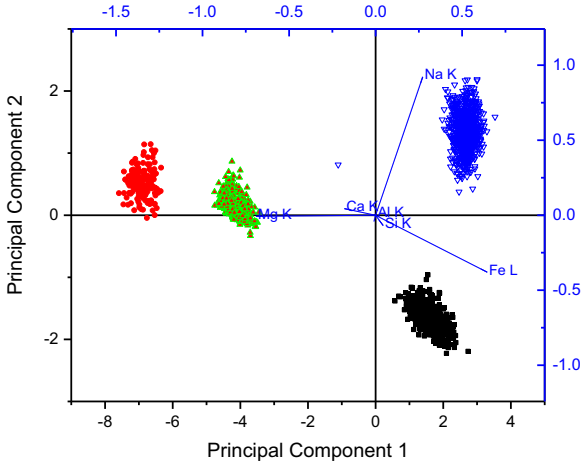

Fig. 5. Principal Component Analysis on classified fibrous asbestos minerals. Chrysotile (red dot), tremolite (green triangle), crocidolite (blue empty triangle), and amosite (black square) were clearly discriminated based on their compositional differences. (For interpretation of the references to color in this figure legend, the reader is referred to the web version of this article.).

several replicates via automated SEM analysis and compared with the expected values, obtained via conventional method. The three asbestos-rich mineral samples from natural outcrops contained both chrysotile and tremolite, as well as deformed veins of coarser-grained antigorite and fragments of tremolite and/or tremolitite that are the most common confounding factors in natural matrix (see Section S1, Supporting information). In all cases, the expected values (Fig. 7, red stars) fell within ± 3σ of the mean (3σ, upper and lower boundaries of the box plots) of the replicated automatic measures. For NOA2 and NOA3, accuracy of result is within 1σ. In real matrix, the precision of the automatic measurement was slightly lower than what obtained with standards, but relative error not exceeded 30% also when only few tens of fibers were detected (raw data in Tab. S11, Supporting information). The concentration of asbestos detected ranged between 10′000 and 500 ppm, indicating that the automatic method could confidently evaluate asbestos in real-case scenarios, in which the boundary between quantitative and semi-quantitative analysis is set to 1000 ppm.

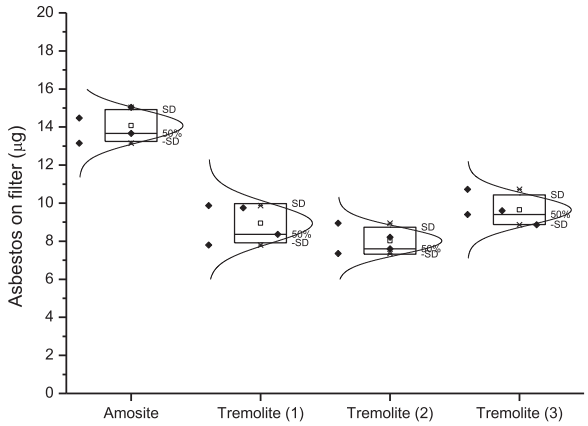

Fig. 6. Evaluation of the precision of the automatic quantitative determination of asbestos. Replicate data (full diamonds) are plotted with box-plot reporting mean values (empty squares), standard deviation (SD), 10th, 90th (asterisks), and 50th percentile.

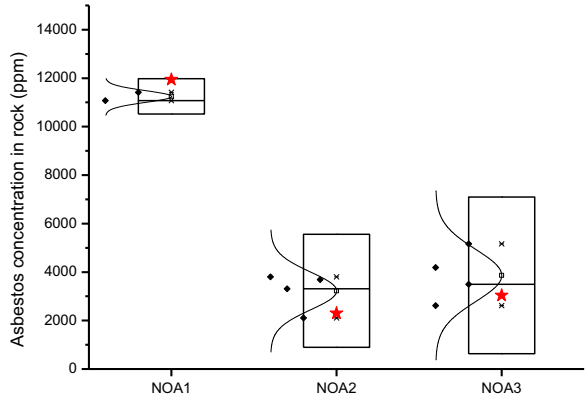

Fig. 7. Evaluation of the accuracy of the automatic quantitative determination of asbestos. Three filters loaded with NOA from complex matrix were quantified with several replicates via automated SEM analysis (box plot, with upper and lower boundaries indicating 3σ) and compared with values (red stars) obtained via conventional method.

3.7. Algorithm flow-chart

The automated method flow may conveniently be sketched with a chart diagram that displays the main phases of the analysis (Section S9, Supporting information). The analysis program starts with a non-recursive calibration step performed on the calibration multi-elemental standard and proceeds to the recursive analysis of the sample(s). The morphometric and the compositional filters discriminate asbestos from non-fibrous amphibole and serpentine minerals, and fibrous minerals. The number of microscopic fields to be analyzed is an input from the user and directly determines accuracy and precision of the analysis (see Section S3.1, in Supporting information) as well as measurement time. By fine-tuning the number of fields to be analyzed, the operator may easily find the best balance between the analytical time/cost and the detection limit of asbestos fibers.

4. Conclusion

To the best of our knowledge, this is the first use of SEM-EDS for a fully automatic quantification of asbestos fibers. The method is meant to quantify asbestos in complex and confounding matrixes, including airborne and waterborne NOA, and amphibole- and serpentine-rich ophiolites. The new method is based on the matched use of the SEM and EDS analytical potentialities, i.e., it identifies the particle shape first and determines the chemical composition later. The proposed automatic method allows quantifying asbestos at low concentration with scalable precision and relies on the combined identification and classification of fibers deposited on a porous membrane by applying a morphometric and a compositional filter. The synergic combination of the filters, discriminates elongated minerals from non-fibrous particles and asbestos from non-asbestiform fibers. The equivalent rectangle (ER) approximation properly estimates width, length, and aspect ratio of non-linear fibers, such as chrysotile, and points out the vast majority of asbestos fibers, up to 94% for UICC crocidolite. The results show an excellent reproducibility and a good precision, when compared to conventional SEM-EDS method. Being fully automated, this procedure significantly enhances the lab productivity and reduces analytical costs. With an analysis time of max 2 h per sample, our method will increase safety for workers and the environment in several occupational settings, including large tunnel excavation in NOA contaminated rocks.

Acknowledgements

Ms S. Fraterrigo-Garofalo's scholarship was kindly funded by ARPA Valle d'Aosta. Ms C. Avataneo is indebted to the "Gronda di Ponente" research project, between University of Torino and SPEA Engineering under the contract no. 400006258/2018, for partially supporting her work. FT thanks Ms. Dunja Lavecchia, Agorà Scienza, University of Torino, for providing the graphical artwork and concept for the Table of Content.

Appendix A. Supporting information

Supplementary data associated with this article can be found in the online version at doi:10.1016/j.talanta.2018.07.083.

References

[1] M. Hendrickx, Naturally occurring asbestos in eastern Australia: a review of geological occurrence, disturbance and mesothelioma risk, Environ. Geol. 57 (2009) 909–926.
[2] R.J. Lee, B.R. Strohmeier, K.L. Bunker, D.R. Van Orden, Naturally occurring asbestos – a recurring public policy challenge, J. Hazard Mater. 153 (2008) 1–21.
[3] F. Turci, S.E. Favero-Longo, C. Gazzano, M. Tomatis, L. Gentile-Garofalo, M. Bergamini, Assessment of asbestos exposure during a simulated agricultural activity in the proximity of the former asbestos mine of Balangero, Italy, J. Hazard Mater. 308 (2016) 321–327.
[4] L. Gaggero, E. Sanguineti, A.Y. Gonzalez, G.M. Militello, A. Scuderi, G. Parisi, Airborne asbestos fibres monitoring in tunnel excavation, J. Environ. Manag. 196 (2017) 583–593.
[5] F. Turci, R. Compagnoni, F. Piana, L. Delle Piane, M. Tomatis, B. Fubini, S. Tallone, S. Fuoco, M. Bergamini, Geological and Analytical Procedures for the Evaluation of Asbestos-Related Risk in Underground and Surface Rock Excavation, in: Engineering Geology for Society and Territory-Volume 5, Springer, 2015, pp. 619–622.
[6] E. Belluso, D. Bellis, E. Fornero, S. Capella, G. Ferraris, S. Coverlizza, Assessment of inorganic fibre burden in biological samples by scanning electron microscopy - energy dispersive spectroscopy, Microchim Acta 155 (2006) 95–100.
[7] National Institute for Occupational Safety and Health (NIOSH), Current Intelligence Bulletin 62: asbestos fibers and other elongate mineral particles: state of the science and roadmap for research, in: D.N. Pubblication (Ed.), 2011.
[8] A. Gualtieri, G. Artioli, Quantitative determination of chrysotile asbestos in bulk materials by combined Rietveld and RIR methods, Powder Diffr. 10 (2013) 269–277.
[9] E. Foresti, M. Gazzano, A.F. Gualtieri, I.G. Lesci, B. Lunelli, G. Pecchini, E. Renna, N. Roveri, Determination of low levels of free fibres of chrysotile in contaminated soils by X-ray diffraction and FTIR spectroscopy, Anal. Bioanal. Chem. 376 (2003) 653–658.
[10] M.-O. Cho, S. Yoon, H. Han, J.K. Kim, Automated counting of airborne asbestos fibers by a high-throughput microscopy (HTM) method, Sensors (Basel Switz.) 11 (2011) 7231–7242.
[11] J. Cherrie, A.D. Jones, A.M. Johnston, The Influence of Fiber Density on the Assessment of Fiber Concentration Using the Membrane Filter Method, Am. Ind. Hyg. Assoc. J. 47 (1986) 465–474.
[12] P.A. Baron, Measurement of airborne fibers: a review, Ind. Health 39 (2001) 39–50.
[13] K. Kawabata, Y. Komori, T. Mishima, H. Asama, An asbestos fiber detection technique utilizing image processing based on dispersion color, Part. Sci. Technol. 27 (2009) 177–192.
[14] I. Zarubiieva, G.B. Hwang, J.S. Lee, G.-N. Bae, Y.-M. Oh, S.-W. Park, T.J. Lee,

H.J. Lee, D.H. Woo, S. Lee, Asbestos imaging and detection with differential interference contrast microscopy, Aerosol Air Qual. Res 13 (2013) 1145–1150.
[15] A.F. Gualtieri, S. Pollastri, N.B. Gandolfi, F. Ronchetti, C. Albonico, A. Cavallo, G. Zanetti, P. Marini, O. Sala, Determination of the concentration of asbestos minerals in highly contaminated mine tailings: an example from abandoned mine waste of Crètaz and Èmarese (Valle d'Aosta, Italy), Am. Mineral. 99 (2014) 1233–1247.
[16] V. Timbrell, R.E.G. Rendall, Preparation of the UICC standard reference samples of asbestos, Powder Technol. 5 (1972) 279.
[17] N. Kohyama, Y. Shinohara, Y. Suzuki, Mineral phases and some reexamined characteristics of the international union against cancer standard asbestos samples, Am. J. Ind. Med. 30 (1996) 515–528.
[18] P. Ballirano, G.B. Andreozzi, G. Belardi, Crystal chemical and structural characterization of fibrous tremolite from Susa Valley, Italy, with comments on potential harmful effects on human health, Am. Mineral. 93 (2008) 1349–1355.
[19] S. Enrico Favero-Longo, F. Turci, M. Tomatis, R. Compagnoni, R. Piervittori, B. Fubini, The effect of weathering on ecopersistence, reactivity, and potential toxicity of naturally occurring asbestos and asbestiform minerals, J. Toxicol. Environ. Health - Part A: Curr. Issues 72 (2009) 305–314.
[20] S.E. Favero-Longo, F. Turci, B. Fubini, D. Castelli, R. Piervittori, Lichen deterioration of asbestos and asbestiform minerals of serpentinite rocks in Western Alps, Int. Biodeterior. Biodegrad. 84 (2013) 342–350.
[21] International Agency for Research on Cancer (IARC), A Review of Human Carcinogens: Arsenic, Metals, Fibres, and Dusts, IARC, Lyon, France, 2012.
[22] A.B. Kane, P. Boffetta, R. Saracci, J.D. Wilbourn, Mechanisms of Mineral Fibre Carcinogenesis, Centre International de Recherche sur le Cancer - IARC, Lyon, France, 1996.
[23] B.W. Case, J.L. Abraham, G. Meeker, F.D. Pooley, K.E. Pinkerton, Applying definitions of "asbestos" to environmental and "low-dose" exposure levels and health effects, particularly malignant mesothelioma, J. Toxicol. Environ. Health Part B Crit. Rev. 14 (2011) 3–39.
[24] W.A. Deer, R.A. Howie, J. Zussman, An Introduction to The Rock-Forming Minerals, Longman, London, UK, 1992.